CRYSTAL GROWTH & DESIGN

Article

pubs.acs.org/crystal

Crystallizing Membrane Proteins in the Lipidic Mesophase. Experience with Human Prostaglandin E2 Synthase 1 and an Evolving Strategy

Dianfan Li,[†] Nicole Howe,[†] Abhiram Dukkipati,[†] Syed T. A. Shah,[†] Benjamin D. Bax,[‡] Colin Edge,[‡] Angela Bridges,[‡] Phil Hardwicke,[‡] Onkar M. P. Singh,[‡] Ged Giblin,[‡] Alexander Pautsch,[§] Roland Pfau,[§] Gisela Schnapp,[§] Meitian Wang,[⊥] Vincent Olieric,[⊥] and Martin Caffrey*[,†]

[†]Membrane Structural and Functional Biology Group, School of Medicine and School of Biochemistry and Immunology, Trinity College Dublin, Dublin 2, Ireland

[‡]Molecular Discovery Research, GlaxoSmithKline, Medicines Research Centre, Gunnels Wood Road, Stevenage, SG1 2PA, U.K.

[§]Departments of Lead Identification and Optimization Support, Boehringer Ingelheim Pharma GmbH & Co. KG, 88400 Biberach an der Riss, Germany

[⊥]Swiss Light Source, Paul Scherrer Institute, Villigen, Switzerland

ABSTRACT: The lipidic mesophase or in meso method for crystallizing membrane proteins has several high profile targets to its credit and is growing in popularity. Despite its success, the method is in its infancy as far as rational crystallogenesis is concerned. Consequently, significant time, effort, and resources are still required to generate structure-grade crystals, especially with a new target type. Therefore, a need exists for crystallogenesis protocols that are effective with a broad range of membrane protein types. Recently, a strategy for crystallizing a prokaryotic α-helical membrane protein, diacylglycerol kinase (DgkA), by the in meso method was reported (*Cryst. Growth. Des.* **2013**, *13*, 2846−2857). Here, we describe its application to the human α-helical microsomal prostaglandin E2 synthase 1 (mPGES1). While the DgkA strategy proved useful, significant modifications were needed to generate structure-quality crystals of this important therapeutic target. These included protein engineering, using an additive phospholipid in the hosting mesophase, performing multiple rounds of salt screening, and carrying out trials at 4 °C in the presence of a tight binding ligand. The crystallization strategy detailed here should prove useful for generating structures of other integral membrane proteins by the in meso method.

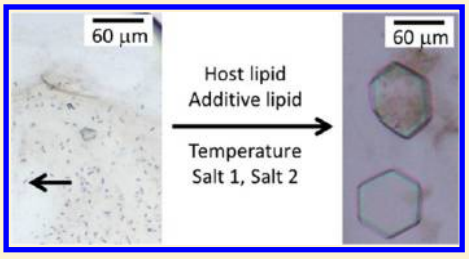

1. INTRODUCTION

Integral membrane proteins serve essential structural, transport, transduction, and enzymatic roles. Defects in membrane protein function are responsible for many debilitating and often fatal diseases. Understanding their mode of action at the molecular level is critical for the development of drugs to treat such diseases. Both processes are greatly facilitated by having available a high-resolution three-dimensional structure of the protein in question. In the case of membrane proteins, structure is most accurately obtained crystallographically. A major challenge in the area of crystallography is the provision of crystals of diffraction quality suitable for high resolution structure determination.

Several methods are available for crystallizing membrane proteins. They can be divided into two major types. The in surfo methods[1] use a detergent solution of the target protein to set up crystallization trials directly. The second method type employs a lipid bilayer for crystallization screening. A variant, referred to as the in meso method, is based on a bicontinuous mesophase.[2] It involves an initial reconstitution of the protein into the lipid bilayer of a cubic mesophase. For this reason, it is also known as the lipid cubic phase (LCP) method. Because crystallization is from a bilayered membrane, the protein is likely to assume a more native and functionally relevant form.

The in meso method made its first appearance 17 years ago.[3] Since then, an impressive array of membrane protein types and complexes has yielded to it, and several have been high profile drug targets. Of particular note is the recent β_2 adrenergic receptor−Gs protein complex structure[4] referred to as "a molecular masterpiece" by the Swedish Academy in its announcement of the 2012 Nobel Prize in Chemistry. That structure was determined using crystals grown by the in meso method.

Despite the fact that the in meso method has been available to the community for almost two decades, until quite recently, uptake in the community has been sluggish. In part, this is due to the viscous nature of the lipidic mesophase which means that handling it requires a few specialty tools, now commercially available, and a little practice. Given its success in providing high resolution structures of important membrane protein targets, the method is now growing in popularity. This is

Received: January 28, 2014
Revised: March 4, 2014
Published: March 7, 2014

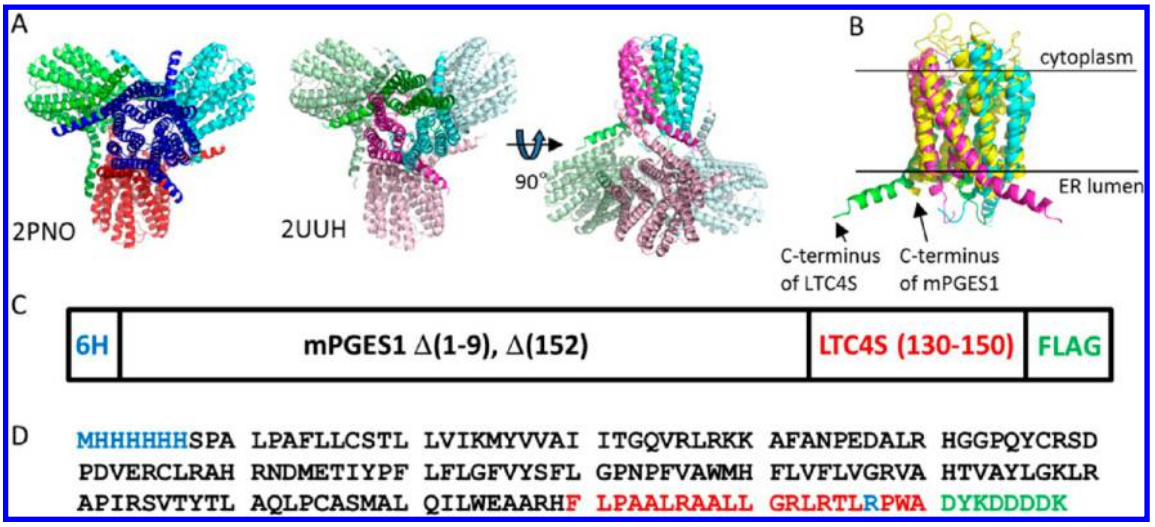

Figure 1. Structure-based rational for design of mPGES1 construct. (A) In two different crystal forms of LTC4S (PDB codes: 2PNO and 2UUH), similar dodecamers are observed. The four trimers, which make up the dodecamer, each sit on the vertex of a tetrahedron and exchange C-terminal extensions with the other three trimers in the dodecahedron. (B) Superposition of the 3.5 Å EM structure of mPGES1 (yellow - PDB code: 3DWW) on a trimer of LTC4S. Note that mPGES1 lacks the C-terminal extension present in LTC4S. (C) The mPGES1* construct used in this study included residues 10−151 of mPGES1 and residues 130−150 of LTC4S (with a Leu to Arg mutation at position 147). A careful comparison suggested this construct might form similar dodecamers to those observed with LTC4S. The construct also includes an N-terminal hexa-His tag and a C-terminal FLAG tag, for purification. (D) The amino acid sequence of the mPGES1* construct is shown.

reflected in the pattern of record entries in the Protein Data Bank (PDB) attributed to the in meso method. Of the 161 records in total to date, 50 have appeared since January, 2012.

In addition to using the method in support of a membrane structural and functional biology program, the Membrane Structural and Functional Biology (MS&FB) Group is active in further developing the technique with a view to bringing it to a wider audience and to making it more generally accessible and useful. The current paper is part of that mission. The target chosen is the human microsomal prostaglandin E2 synthase 1 (mPGES1), a 17 kDa α-helical trimer that catalyzes the glutathione (GSH)-dependent isomerization of prostaglandin H2 (PGH2) to PGE2.[5] A high resolution in surfo crystal structure of this enzyme was published[6] three months after we had solved its structure to 2.08 Å by the in meso method. The in meso work was done with crystals grown following a strategy developed based on experience with other integral membrane protein targets.[7,8] However, to obtain a final high resolution structure additional screening and optimization approaches were needed. These included adjusting the host and additive lipids that create the mesophase from which crystals grew, multiple rounds of salt screening, and performing trials at 4 °C in the presence of a tight binding ligand. In addition, the protein was engineered to include an extramembrane C-terminal extension for crystal contact formation. The many rounds of screening and optimization implemented and their outcomes are detailed here along with an explanation for why they were used and why they did or did not work. The crystallization strategy described should prove useful for generating structures of other integral membrane proteins by the in meso method.

2. MATERIALS AND METHODS

2.1. Materials. Monoolein (9.9 MAG (monoacylglycerol; MAG nomenclature is described in ref 9), lots M239-F15-U, M239-M27-U) and monopalmitolein (9.7 MAG, lot M219-J5-W) were purchased from Nu-Chek Prep (Elysian, MN). 7.7 MAG (lot TasB74), 7.8 MAG (lots Tas53), 8.8 MAG (lot TasC15 and Tas23), 8.9 MAG (lot ACN17), and 7.9 MAG (lot ACN11) were synthesized and purified in-house following established procedures.[10,11] Sodium hydroxide (Cat. S8045, lot SZBC1290V), 2-methyl-2,4-pentanediol (MPD) (Cat. 68340, lot 1261783 32007025), L-glutathione reduced (Cat. S4251, lot 060M1762V), SIGMAFAST Protease inhibitor cocktail tablet, EDTA-free (Cat. S8830, lot SLBC2622V), EGTA (Cat 03777, lot 0001426960), EDTA (Cat. E5135, lot 087K0049), Triton X-100 (Cat T9284, lot MKBF3557V), imidazole (Cat I0250, lot 068K5303), HEPES (Cat H4034, lot SLBF8768V), sodium phosphate monobasic (cat S8282, lot 054K01431), and sodium phosphate dibasic (Cat S9763, lot BCBF5244V) were obtained from Sigma (St. Louis, MO). 1,2-Dioleoyl-*sn*-glycero-3-phosphocholine (Cat 850675P, lot 181-271) was purchased from Avanti. Sodium chloride (Cat. BP358-1, lot 107174) was obtained from Fisher Scientific (Loughborough, UK). *n*-Decyl-β-D-maltopyranoside (DM, Cat. D322, lot 126862) was purchased from Affymetrix Anatrace (Santa Clara, CA). Glycerol (Cat. G1345, lot C22500) was from Melford Laboratories (Ipswich, UK). Ni-NTA resin (Cat. 1018142, lot 142315549) was from Qiagen (Hilden, Germany). Amicon ultracel 50K concentrators (Cat. UFC505096, lot R1EA80242, Cat. UFC805024, lot R2EA14395, Cat. UFC905024, lot R2EA14388) were from Millipore. Gas-tight Hamilton syringes 100 μL (Cat. 7656-01, model 1710 RN SYR) were obtained from Hamilton. Lonza PAGEr Gold Precast gels 12%, 10 cm × 10 cm, 16 wells, thickness 1 mm (Cat. 59515, lot 0000311656-019) were purchased from Lonza (Basel, Switzerland). *N*-(2-Acetamido)-iminodiacetic acid (ADA) solution (Cat. HR2-507, lot 250721, 250722) was purchased from Hampton Research (Aliso Viejo, California). Crystallization screens: Crystal Screen HT (Cat. HR2-130, lot 211094), Index HT (Cat. HR20144, lot 214407), and MemFac HT (Cat. HR2-137, lot 213103-24-22); as well as optimization screens: StockOption Salt (Cat. HR2-245, lot 224508), StockOption pH screen (Cat. HR2-241, lot 224111), and Additive Screen HT (Cat. HR2-138, lot 213803), were purchased from Hampton Research (Aliso Viejo, CA); JBScreen Membrane HTSS (Cat. JBS 00011630, lots 2004/01 and 2003/02) was from Jena Bioscience GmbH (Jena, Germany); MemGold (Cat. MD1-39, lot 004-1-39), HT96 PACT Premier (Cat. MD1-36, lot BN002) and MemStart & MemSys (Cat. MD1-33, lot 011121) were from Molecular Dimensions (Newmarket, Suffolk, UK); Cubic Screen (Cat. CS-EB-LCP-B, lot CEB5-BLCP), Wizard I, II and III (Cat. EBS-WIZ-1/2/3, lot EBS 0006152009299) were from Emerald Biosystems (Bainbridge Island, WA); Mbclass (Cat. 130711) was obtained from

Qiagen (Hilden, Germany). Superdex 200 16/60 was from GE Healthcare (Little Chalfont, Buckinghamshire, UK).

2.2. Methods. *2.2.1. Cloning and Expression.* Residues 10−151 of mPGES1 (GenBank Accession number NM_004878) were amplified by PCR using the following primers, forward primer: 5′- GATCG-ATCGGATCCATGCACCATCACCATCACCATCCTGCCCACA-GCCTGGTG-3′; first reverse primer: 5′-GTCGATCTCGAGTCA-TGCCCAAGGCAGTAATGTACGTAGACGTCCCAATAA-TGCAGCGCGCAGTGCAGCTGGCAGAAAGTGGCGGGC-CGCTTCCCAGAG-3′; and second reverse primer: 5′-GATCGATCTCGAGTCACTTATCGTCGTCATCCTTGTAA-TCTGCCCAAGGACGTAATGTACG-3′. An unintended error in primer synthesis (A−C, italic) introduces a point mutation, L147R. The PCR product was digested with *BamH*I and *Xho*I (restriction sites underlined in the forward and second reverse primer, respectively) and subcloned into the pFASTBAC1 vector (Invitrogen) cut with the same restriction enzymes. The resulting construct contained the coding sequence for a hexa-His tag followed by residues 10−151 of mPGES1, residues 130−150 of LTC4S containing an L147R point mutation, and a FLAG tag (Figure 1D). The plasmid was transposed into the baculovirus genome using BAC-to-BAC technology (Invitrogen). The resulting recombinant Bacmid DNA was transfected into *Spodoptera frugiperda* (*Sf*9) cells using Cellfectin II (Invitrogen) to generate virus.

*Sf*9 insect cells were grown in suspension in serum-free ExCell 420 medium (Cat. 14420C, Sigma) at 27 °C. Cells were initially seeded and grown and maintained in 2 L flasks (Corning Erlenmeyer) and later inoculated to 50 L wave bags (Wave Biotech) supplied with filtered air at 2 L/min to ensure oxygenation. Cells in the wave bags, seeded at ∼4×10^5 viable cells/mL, were allowed to grow for 3 days to a density of ∼3×10^6 viable cells/mL before infection with baculovirus at a multiplicity of infection of 3. Forty-eight hours after infection, cells were pelleted by centrifugation for 30 min at 2500*g* and 4 °C (CARR Viafuge). The resulting cell slurry was transferred to Bioprocessing Liners (Beckman Coulter) and centrifuged for 20 min at 2500*g* and 4 °C. After the supernatant was removed, the cell pellet (∼310 g wet weight per 50 L bag) was stored at −80 °C until use.

2.2.2. Protein Purification. Cells (10 g) were thawed in 50 mL of Buffer A (0.3 M NaCl, 10% (v/v) glycerol, 2 mM reduced glutathione (GSH), 1 mM EDTA, 1 mM EGTA, protease inhibitor (1 mg/L, Cocktail Set III, Cat. 539134, Merck Biosciences) and 20 mM sodium phosphate pH 8.0) by gentle stirring at 4 °C for 30 min. Cells were broken using a probe sonicator at 4 °C for 10 min with a "0.5 s on−0.5 s off" duty cycle and a power setting of 30% (model HD2200, Probe KE76, Bandelin). To the lysate was added 50 mL of Buffer A supplemented with 8% (v/v) Triton X-100, providing a final concentration of 4% (v/v) detergent in the solubilization buffer. All subsequent steps were carried out at 4 °C unless otherwise noted. After 90 min of mixing at 10 rpm on a Stuart SB3 rotator (Bibby Scientific), the solubilized protein was separated from cell debris and insoluble material by centrifuging the detergent-treated lysate at 48000*g* for 1 h (Rotor SS34, Sorvall). The supernatant was diluted into 0.5 L of Buffer B (0.3 M NaCl, 10% (v/v) glycerol, 2 mM GSH, 20 mM imidazole, 20 mM sodium phosphate, pH 8.0) and combined with 10 mL of Ni-NTA resin pre-equilibrated with Buffer B. After 16 h incubation at 10 rpm on a SB3 rotator, the resin was placed in a gravity flow column (Cat. 732-1010, Bio-Rad). The resin was washed with 0.15 L of Buffer C (0.2% (v/v) Triton X-100, 0.3 M NaCl, 10% (v/v) glycerol, 2 mM GSH, 20 mM imidazole, and 20 mM sodium phosphate pH 8.0). The Triton X-100 detergent was exchanged to *n*-decyl *β*-D-maltoside (DM) by washing the column with 0.4 L of Buffer D (0.25% (w/v) DM, 0.3 M NaCl, 10% (v/v) glycerol, 2 mM GSH, 20 mM imidazole, 20 mM sodium phosphate pH 8.0). Protein was eluted with 0.3 M imidazole in Buffer D. The eluate (∼10 mL) was split in two and gel filtered on a Superdex 200 16/60 column equilibrated with gel filtration buffer (0.25% (w/v) DM, 0.2 M NaCl, 2 mM GSH, 10% (v/v) glycerol, 20 mM HEPES pH 7.5) attached to an AKTA FPLC system (GE Healthcare). The protein came off the column with an elution volume (V_e) of 69.1 mL as a symmetric peak. Peak fractions from the two runs were pooled (∼12 mL total at 0.55 mg/mL) and concentrated to 20−80 mg/mL using a concentrator (Amicon Ultracel-50 membrane, Cat. UFC905008, Millipore). Purity was assessed by SDS-PAGE at 20 °C without preheating the sample using Coomassie Blue as the stain.[8]

2.2.3. Mass Spectrometry. To confirm protein identity, bands were excised from Coomassie-stained SDS-PAGE gels with a clean blade. The matrix was sent to Aberdeen Proteomics for extraction, tryptic digestion, and mass spectrometric (MS) analysis using MALDI-TOF. To further investigate the integrity of the protein, two types of MS analysis were carried out. In the first, the sample, purified in DM detergent, was diluted into 0.1% (v/v) trifluoroacetic acid and was subjected to MALDI-TOF MS (Aberdeen Proteomics, University of Aberdeen, UK). In the second, the protein (0.1 mg) was precipitated using 0.5 mL of 15% (w/v) trichloroacetic acid at room temperature (RT, 20−21 °C). The white precipitate was washed three times with Milli-Q water. After air-drying, the sample was sent to the Astbury Center for Structural Molecular Biology (University of Leeds, UK) for liquid chromatograph mass spectrometric analysis (LC-MS/MS).

2.2.4. Crystallization. In meso crystallization trials began with an initial reconstitution of the protein into the bilayer of the lipid mesophase. This was performed following a standard protocol.[12] The protein solution containing 10−40 mg of mPGES1*/mL was homogenized with monoolein (9.9 MAG) in a coupled syringe mixing device[13] at RT using two volumes of protein solution and three volumes of lipid. For 7.7 MAG, 7.8 MAG, and 8.7 MAG, which have slightly different phase behaviors compared to monoolein, the volume ratio used was 1:1. With 7.9 MAG, 8.8 MAG, 8.9 MAG, and 9.7 MAG, the corresponding cubic phases were prepared as for monoolein. When dioleoyl phosphatidylcholine (DOPC) was to be included, the phospholipid was added either directly to the protein solution, as a dry powder, at 3 mg/mL, or it was doped into the MAGs using a published procedure[14] at 0.5−5 mol % with respect to the host lipid. Ligands, when used, were added to the protein solution at a final concentration of 7 mM from a 0.2 M stock in dimethylsulfoxide. The ligands did not dissolve fully in the protein solution. Regardless, the protein solution with precipitated ligand was used for mesophase preparation, as described above. Following this protocol, an optically clear, protein-laden mesophase was obtained consistent with the ligand having partitioned into the protein and/or the mesophase.

Crystallization trials were set up by transferring 50 nL of the protein-laden mesophase onto a silicanized 96-well glass sandwich plate followed by 0.8 μL precipitant solution using an in meso robot.[12,15] Commercial screens, diluted to various degrees,[8] were used for the initial screening. The glass plates were stored either in a walk-in cold room at 4−6 °C or in an incubator/imager at 20 °C (RockImager RI1500, Formulatrix, Inc., Waltham, MA) for crystal growth. Crystallization progress was monitored automatically in the imager and manually using normal and polarized light microscopy (Eclipse E 400 Pol and Nikon Digital Sight DS-Fi2). Crystals from the lipidic cubic or sponge phases were harvested and snap-cooled, as described.[16]

2.2.5. Data Collection, Structure Determination, and Refinement. Native data sets were collected on beamlines 23ID-B at the Advanced Photon Source (APS), I24 at the Diamond Light Source (DLS), and PX II (X10SA) at the Swiss Light Source (SLS). At the APS, data were collected with a 1° oscillation and a 1 s exposure per image, a collimated beam size of 10 × 10 μm^2, and a sample-to-detector distance of 400 mm, with a MAR 300 CCD detector using 1.033 Å X-rays. At the DLS, data were collected with a 0.2° oscillation and a 0.2 s exposure per image, a microfocus beam size of 10 × 10 μm^2 and a sample-to-detector distance of 500−600 mm, with a Pilatus 6 M detector using 0.978 Å wavelength X-rays. At the SLS data were collected with a 0.1° oscillation and a 0.1 s exposure per image, a collimated beam size of 30 × 10 or 15 × 10 μm^2 and a sample-to-detector distance of 350 mm, with a Pilatus 6 M detector using 1.033 Å X-rays. The structure was solved by sulfur-SAD (single wavelength anomalous diffraction) with data collected at 2.066 Å wavelength (6 keV) at SLS beamline PXIII (X06DA) with a 0.1° oscillation and a 0.1 s exposure per image on a PILATUS 2M detector. Two crystal orientations obtained by means of a multiaxis goniometer PRIGo were used to reduce systematic measurement errors (4 × 360° at Chi = 0°

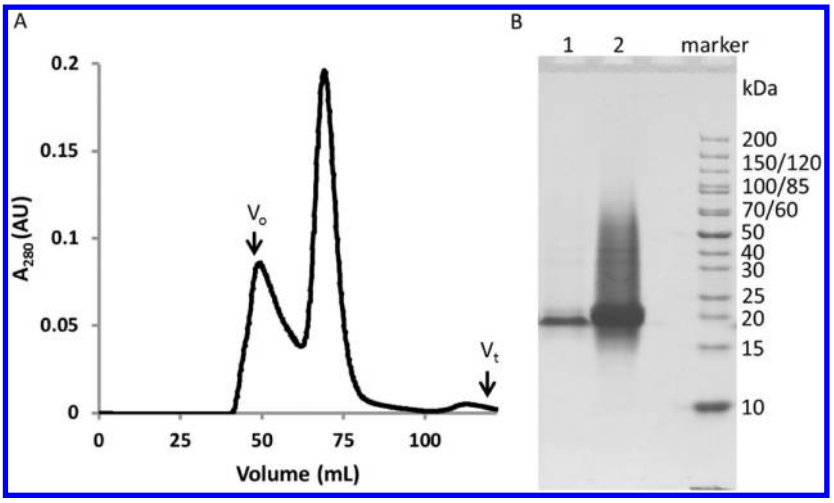

Figure 2. Purification of mPGES1*. (A) Size exclusion chromatographic analysis. V_o and V_t mark the void and total column volumes, respectively. The void volume peak likely represents aggregated protein. The elution volume (V_e) for mPGES1* is 69.1 mL, which corresponds to an apparent molecular weight of 126 kDa. The near Gaussian shaped elution profile is consistent with a protein that is monodisperse. (B) SDS-PAGE analysis of mPGES1* from the mPGES1* peak in the chromatogram in (A) visualized using Coomassie Blue stain. Lanes 1 and 2 represent 4 and 40 μg of protein, respectively. The purpose of the low loading used in Lane 1 was to reveal contaminant bands that might overlap with the major band. Indeed, a very faint band was observed above the main mPGES1* band at ~19 kDa. High loading in Lane 2 was used to reveal minor contaminants that otherwise might go undetected. The smear seen on either side of the main mPGES1* band in lane 2 is likely due to high levels of DM in the sample loaded on the gel. DM may compete with SDS for binding sites on mPGES1* producing a sample with a protein charge/mass range that shows up as a smear. Molecular weight markers are in lane 3. The sample is estimated to have a purity of >95%. The protein migrates as a monomer at the expected molecular weight of ~18 kDa.

and 2 × 360° at Chi = 15° corresponding to a total of 2160°). Data were processed using XDS,[17] XSCALE and AIMLESS.[18] Substructure was solved using SHELXD,[19] followed by substructure refinement and phasing with PHASER,[20] and density modification with DM.[21] Model building was performed using BUCCANEER[22] and COOT.[23] The final model was refined against the high resolution native data set (2.08 Å) using PHENIX.[24]

3. RESULTS

3.1. Construct Design. The initial mPGES protein construct with a hexa-His at the N-terminus and a FLAG tag at the C-terminus failed to crystallize in surfo when trials were conducted in the presence of glutathione (GSH) or various inhibitors. Consequently, the structures of members of the MAPEG family (membrane associated proteins in eicosanoid and glutathione metabolism)[25] available in the Protein Data Bank (PDB) at the time were examined for ideas as to how to rationally design in crystal contacts. Four relevant records were found. Two, that included mPGES1 (PDB entry 3DWW, 3.5 Å)[5] and the microsomal glutathione *S*-transferase 1 (mGST1, PDB entry 2H8A, 3.2 Å),[26] referred to structures solved by electron crystallography. The other two were X-ray crystal structures that included 5-lipoxygenase activating protein (FLAP, PDB entries 2Q7R, 2Q7M) and leukotriene C4 synthase (LTC4S, PDB entries 2UUI, 2UUH,[27] 2PNO[28]) at ~4.0 Å[29] and ~2 Å resolution, respectively. The highest resolution structures available, at that time, were of LTC4S. Examination of LTC4S crystal structures showed that in two different space groups similar dodecamers were formed (Figure 1A). Comparison of the LTC4S crystal structures and the mPGES1 EM structure then available (PDB entry 3DWW) suggested that by fusing the C-terminal helix from LTC4S onto mPGES1 it might be possible to induce mPGES1 to form similar dodecamers (Figure 1), facillitating crystallization. Nine residues at the N-terminus of mPGES1 were disordered in the electron crystallographic structure and accordingly were not included in the construct. A hexa-His and a FLAG tag was added to the N- and C-termini, respectively, to facilitate purification and detection. The components of this construct, hereafter referred to as mPGES1*, are shown in Figure 1.

3.2. Protein Purification and Identification. mPGES1*, expressed in high yield in *Sf*9 insect cells, was solubilized in Triton X-100 and purified in this detergent by Ni-NTA. The Triton X-100 was exchanged to DM on the Ni-NTA column, and the protein was further purified using size exclusion chromatography. The size exclusion chromatogram shows a major Gaussian-shaped peak with an elution volume corresponding to a protein-detergent complex with an apparent molecular weight (MW) of 126 kDa. A void volume peak suggested that the Ni-NTA purified sample contained sizable amounts of aggregated protein. Relevant fractions from the included volume peak were collected, concentrated to 80 mg/mL, and subjected to SDS-PAGE analysis with Coomassie Blue staining (Figure 2B). A major band with an apparent MW of 18 kDa was observed suggesting that the protein, with a calculated monomeric MW of 20.5 kDa, was monomerized in SDS and that the protein had a purity of >95%. Given the purity and performance of the sample, no further purification procedures (FLAG tag, ion exchange, etc.) were used. The typical yield was 6−7 mg of pure protein from 10 g cells.

To verify the identity of the protein as mPGES1, the protein from the 18 kDa band was extracted from the SDS-PAGE and analyzed by MALDI-TOF. Three fragments were identified with observed MWs (calculated based on experimental mass/charge ratio) of 1102.54 Da (expected MW 1102.66, MYVVAIITGQVR with oxidized Met), 1364.75 Da (expected MW 1364.92, KAFANPEDALR) and 2692.37 Da (expected MW 2692.49, SVTYTLAQLPCASMALQILWEAAR). These values are consistent with the analyzed protein containing part or all of mPGES1*. Additional MALDI-TOF and LCMS-MS analyses provided total MW values of 20328.30 and 20327.69

dx.doi.org/10.1021/cg500157x | *Cryst. Growth Des.* 2014, 14, 2034−2047

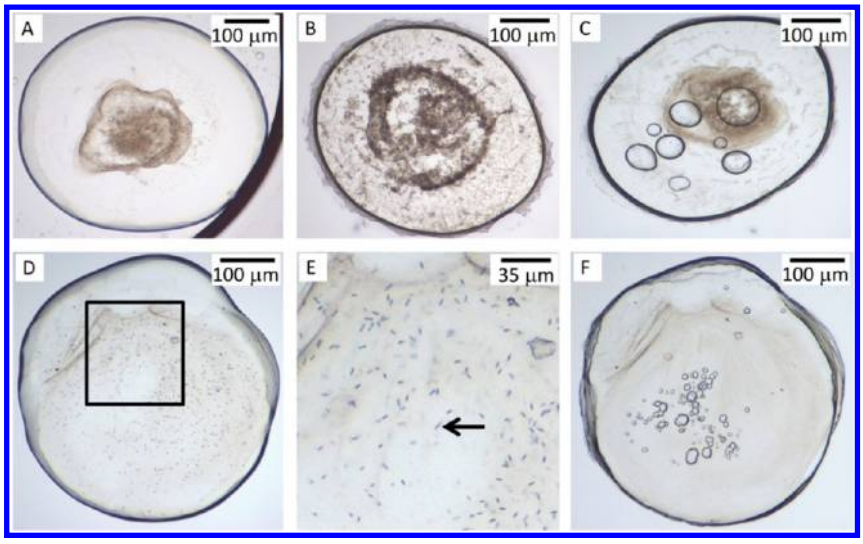

Figure 3. Results of in meso crystallization trials with mPGES1*, illustrating the critical role of the additive lipid, DOPC, in generating the first crystal hits. Neither 9.9 MAG (A) nor 7.8 MAG (B), as host lipids, produced crystals in the absence of DOPC. Combining DOPC with the protein prior to reconstitution into the 9.9 MAG-based mesophase had no effect on crystallization (C). Doping 9.9 MAG with 5 mol % DOPC prior to mesophase formation and reconstitution produced microcrystals (D). An expanded view of the boxed area in (D) is shown in (E). A microcrystal, measuring ~5 um in maximum dimension, resides at the tip of the arrow. In the absence of GSH, the crystals in (D) and (E) disappeared after 3 to 7 days (F). All trials were conducted at 20 °C using a precipitant solution that included 7.8% (v/v) MPD and 70 mM ADA pH 6.5.

Da, respectively, consistent with a theoretical MW of 20328.86 Da with the N-terminal methionine intact. Combined the size exclusion chromatography, SDS-PAGE and MS results indicated that the protein sample was monodisperse and relatively pure, consisted of mPGES1* as designed (Figure 1C), and thus was suitable to enter crystallization trials.

3.3. Initial Trials and Preliminary Optimization. *3.3.1. DOPC Was Critical for Obtaining Initial in Meso Crystals.* Initial in meso crystallization trials were set up at 20 °C with monoolein (9.9 MAG) as the host lipid and with mPGES1* at 20 mg/mL in the presence of 2 mM GSH. Of the 1008 conditions screened in "duplicate", no hits were observed [The screens used included ten and a half 96-well blocks listed in section 2.1. Precipitant solutions were either used directly without dilution or diluted to varying percentages of full strength with Milli-Q water as follows: PACT premier, 65%; MemGold, Mbclass, MemSys & MemStart, Wizard I, II & III, MembFac and Index, 70%; and JBScreen Membrane HTSS, 80%. For each screen, trials were set up in the forward and reverse direction as "duplicates," as described in ref 7]. Instead, the mesophase bolus remained optically clear or, in the case of some MPD-containing precipitants, developed a brownish hue corresponding to precipitated or possibly microcrystalline protein (Figure 3A). Repeating the entire screening process with 10 mM GSH had no effect.

In previous work with a β-barrel porin[7] (OprB from *Pseudomonas aeruginosa*) and an α-helical kinase[8] (DgkA from *Escherichia coli*), screening with alternative, short chain host lipids proved successful in generating quality crystals and high resolution structures. This strategy was therefore applied to mPGES1*. 7.8 MAG was investigated initially as this is what worked with the kinase, which like mPGES1*, is a small, hydrophobic α-helical trimer. Unfortunately, no crystal hits were observed, and the MPD-containing conditions often produced a heavy precipitate (Figure 3B).

Additive lipids can have a profound effect on crystallogenesis. In the case of the GPCR family of membrane receptors, cholesterol has been used to great effect;[2] usually combined with the host lipid, monoolein, to the extent of 8−12 mol %. mPGES1 resides in the endoplasmic reticulum which is rich in phosphatidylcholine (PC).[30] We speculated that this would be an appropriate additive lipid. And so trials were set up using protein solution to which was added dioleoylphosphatidylcholine (DOPC) at 3 mg/mL corresponding to 3.8 mol of DOPC per mole of mPGES1*, alas to no effect. As before, a brown precipitate developed particularly in MPD-based conditions (Figure 3C).

It was reasoned that the level of PC doping might not have been enough in these initial crystallization trials. Should the added PC partition completely into the host lipid, on average each PC molecule would be associated with 1000 molecules of monoolein. To further increase the PC loading however, it was necessary to do so by combining it with the monoolein prior to mesophase preparation. This was done, bringing the DOPC concentration to 5 mol %, and for the first time crystal hits were obtained. The 5 μm-sized crystals were obtained after 4 h at 20 °C under conditions (7.8% (v/v) MPD, 70 mM ADA pH 6.5) that previously had produced brown precipitate. They stopped growing after a day (Figure 3D,E).

An attempt to optimize the conditions was undertaken by screening MPD concentration from 5 to 15% (v/v) in increments of 1%. In addition, butanediol was evaluated as an alternative to MPD and was tested in the range 10−25% (v/v), and MES and Bis-Tris buffers were examined as alternatives to ADA. Crystals were obtained at 6−10% (v/v) MPD with 8% (v/v) as the optimum. Butanediol did not substitute for MPD in the conditions tested. And ADA could be replaced with MES or Bis-Tris but without a significant improvement in crystal quality, as judged by eye. Overall, this initial round of optimization did not lead to better looking crystals, and the conditions that produced the initial hits became the reference for further work.

3.3.2. GSH Is Essential to Stabilize mPGES1 Crystals. Under reference conditions, crystals disappeared between 3 and 10 days postsetup (Figure 3F). Given that GSH is a cofactor for mPGES1[5] and its susceptibility to oxidation,[31] we suspected

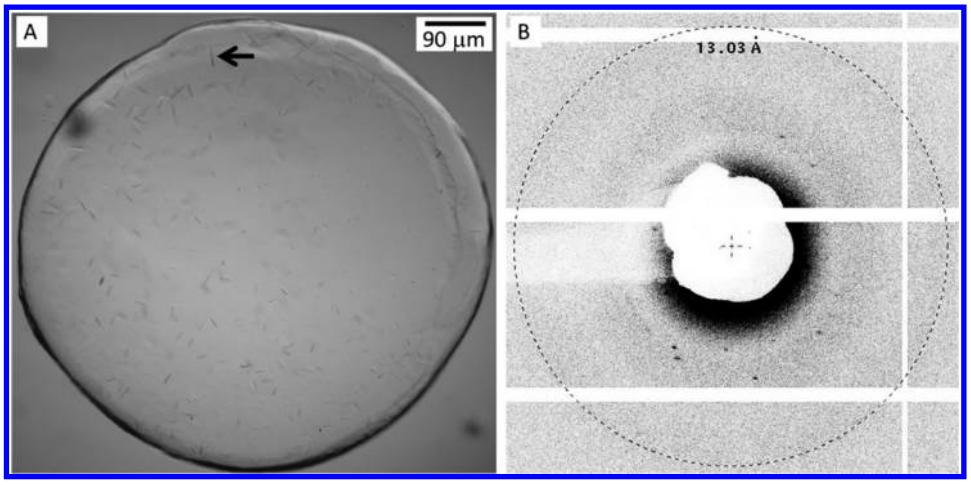

Figure 4. Image of and first diffraction from mPGES1* crystals. (A) Crystals grown at 4 °C. Compared to crystals at 20 °C, considerably less precipitated protein, which appears as a brownish aggregate (see Figure 3D), was observed at 4 °C. The precipitant solution included 3% (v/v) hexanediol, 7.8% (v/v) MPD, and 70 mM ADA pH 6.5. 9.9 MAG doped with 5 mol % DOPC was used to form the mesophase. (B) Diffraction from crystals in (A) recorded with the unattenuated, 10 × 10 μm^2 beam at beamline I24, Diamond Light Source. The sample-to-detector distance was set to 700 mm. The sharp reflections in the ∼20−40 Å region of the diffraction pattern, while sparse, are consistent with scattering from a crystal of a macromolecule and suggest that mPGES1* had been successfully crystallized.

that a reduction in GSH concentration over time due to diffusion from the mesophase into the bathing precipitant solution and to oxidation may have been responsible for crystal instability. By supplementing the precipitant solution with GSH to the same concentration (2 mM) as that used in preparing the protein solution, the reduction in GSH concentration due to dilution was avoided. This had the effect of producing crystals that were stable in the mesophase for at least a month. For all future work, both the protein solution and all precipitants solutions contained 2 mM GSH. The noted sensitivity of the crystals to GSH concentration was consistent with the crystals being mPGES1* as opposed to being composed of salt, detergent, or lipid. This finding, in conjuction with the observed reproducibility of the crystallization experiment, indicated that the new condition was worthy of further optimization.

3.4. Optimization. *3.4.1. Temperature, Salt, and Additive Screening.* Early on in any trial, a screen of temperature is performed as soon as reproducible crystallization conditions have been established. With DgkA, for example, significant improvements in crystal size and diffraction quality were observed when crystallization was done at 4 °C.[8] Further, with mPGES1* initial hits consisted of showers of microcrystals in the presence of what looked like precipitated protein, and the process was rapid taking place over the course of hours to a few days. Slowing down the process by lowering temperature was therefore considered a very reasonable way forward. Accordingly, trials were set up under reference conditions (20 mg mPGES1*/mL, 5 mol % DOPC in monoolein, 2 mM GSH, 8% (v/v) MPD, 70 mM ADA pH 6.5) at 20 °C, and the plates were incubated at 4 °C for crystal growth. As expected, the mesophase did not transform to the solid state reflecting, no doubt, its pronounced ability to undercool and to remain in a metastable state for extended periods.[32] In addition to evaluating the effect of low temperature, a salt and additive screen was carried out as part of this round of optimization. Thus, on top of the basic precipitant solution consisting of 2 mM GSH, 8% (v/v) MPD, and 70 mM ADA pH 6.5, salts were added to a final concentration of 0.1 and 0.4 M (Hampton Research HR2-245), and additives were added to 10% of the values in the Hampton Research HR2-138 additive kit.

A typical well for low temperature crystallization of mPGES1* is shown in Figure 4A. As noted, the bolus did not solidify, consistent with the mesophase remaining in a metastable, undercooled state at 4 °C. Further, there were considerably fewer and larger (∼30 μm sized needles) crystals than observed at 20 °C (Figure 3D). The brown precipitate, a common feature at 20 °C, was much less in evidence at 4 °C. Overall, the contrasting behavior of mPGES1* at 4 and 20 °C is very similar to that observed with DgkA.

Interestingly, this round of optimization did not reveal further improvements in mPGES1* crystallization attributable to added salts or additives. Subsequently, we discovered that the trials had been performed at suboptimal pH, a topic to which we will return (section 3.4.2).

At this point in the screening exercise, we planned to further optimize on the basis of host lipid identity. However, because host lipids are expensive and indeed some had to be synthesized and purified in-house, it was deemed important to verify that the crystals observed to date were proteinaceous. Accordingly, crystals were harvested (Figure 4A) and tested for diffraction on the microfocus beamline at the Diamond Light Source (Didcot, UK). The diffraction pattern, with a few sharp reflections out to about 20 Å (Figure 4B), provided convincing evidence that we were dealing with protein crystals and that further optimization was in order.

3.4.2. Host Lipid, Salt, Additive and pH Screening. Six different MAGs (7.7, 7.8, 8.8, 8.9, 7.9, and 9.7 MAG), all doped with 5 mol % DOPC, were used for the host lipid screen. Three precipitant solution screens, for use in combination with the different host lipids, were rationally designed, based mainly on our experience with a similar trialing of DgkA,[8] as outlined below. All screen solutions contained 2 mM GSH.

(i) MPD - Fine pH Grid Screen. This 96-condition screen included eight MPD concentrations ranging from 3.5 to 10.5% (v/v) in 70 mM ADA buffer and covered 12 pH values in the range from pH 5.7 to 7.9 in increments of 0.2 pH units. As already noted, 8% (v/v) was the optimum MPD concentration with monoolein as the host lipid (section 3.3.1). The reason for

dx.doi.org/10.1021/cg500157x | Cryst. Growth Des. 2014, 14, 2034−2047

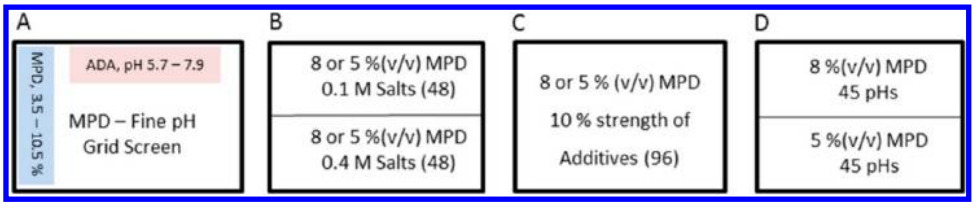

Figure 5. Make up of screens used for optimizing mPGES1* crystallization. All screens contained 2 mM GSH and 70 mM ADA pH 6.5, unless otherwise indicated. (A) The MPD-Fine pH Grid screen. In a 96-well plate, pH was increased in 0.2 pH unit increments from 5.7 in column 1 to 7.9 in column 12. In the same plate, MPD concentration (% (v/v)) was increased from 3.5 in row 1 to 10.5 in row 8 in increments of 1% (v/v). (B) The 48 salts (1−48#) in Hampton Research HR2-245 salt screen kit were added to the basic condition with either 5 or 8% (v/v) MPD to the extent of 0.1 M (wells A1-D12) and 0.4 M (wells E1-H12), resulting two 96-well screens. (C) The 96 additives in the Hampton Research HR2-138 additive screen kit were doped into the basic crystallization condition with 5 or 8% (v/v) MPD to the extent of 10% of their original concentrations, resulting two 96-well screens. (D) The 45 buffers/pH combinations in the Hampton Research HR2-241 buffer/pH screen kit, covering a pH range from 2.2 to 11.0, were added to the basic conditions (5 or 8% (v/v) MPD) to a final concentration of 0.1 M, resulting in a 90-condition screen.

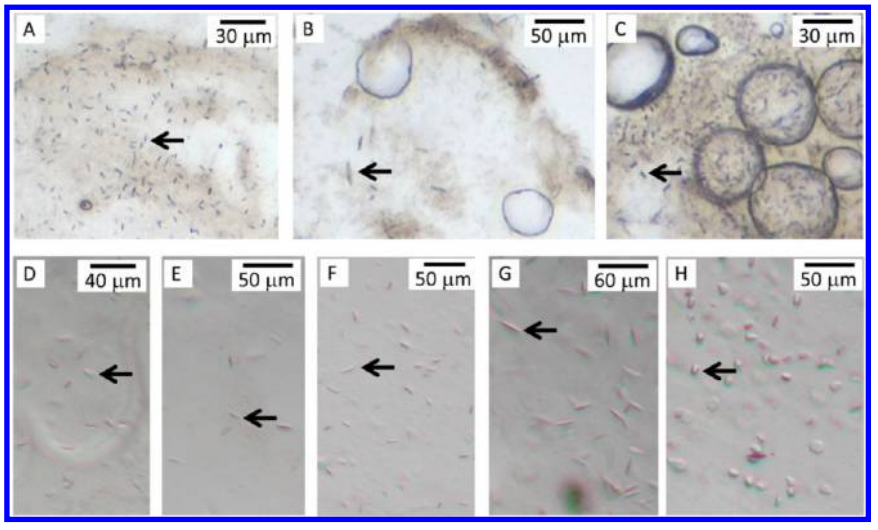

Figure 6. Impact of host lipid, pH, and temperature on the crystallization of mPGES1*. (A) 7.8 MAG at 20 °C. (B) 9.7 MAG at 20 °C. (C) 8.8 MAG at 20 °C. (D) 7.9 MAG at 4 °C. (E) 9.7 MAG at 4 °C. (F, G, and H) 8.8 MAG at 4 °C. All host lipids were doped with 5 mol % DOPC. The precipitant solution contained 2 mM GSH, 3.5−8% (v/v) MPD and 70 mM ADA pH 6.5 (A−F), pH 6.7 (G) or pH 7.1 (H). In 8.8 MAG, crystals were smaller, but with more three-dimensional bulk, at pH 7.1 (H) than at pH 6.5 or pH 6.7. Images were recorded 5 days postsetup. Typical crystals in each image are indicated by arrows.

extending the screen all the way to 3.5%(v/v) MPD has its origins in our experience with DgkA where the optimum MPD concentration was found to shift to lower values with the shorter chain MAGs.[8] This difference in behavior was expected to be adequately covered in the proposed 3.5−10.5% (v/v) MPD range for use with the six MAGs that varied in acyl chain length from 14 to 17.

(ii) Salts and Additive Screens. Two sets of 96-condition screens were designed to evaluate crystallization dependence on salts and additives. The two differed in MPD concentration chosen for optimal compatibility with the shorter and longer chained MAGs. Thus, for the longer chain MAGs (≥16 C) that included 8.8, 8.9, 7.9, and 9.7 MAG, screens were prepared with 8% (v/v) MPD. For the shorter chain MAGs, which included 7.7 and 7.8 MAG, screens contained 5% (v/v) MPD. The actual concentrations chosen again were based on prior experience with DgkA. All screens included 70 mM ADA buffer pH 6.5. The salt screens were prepared in the MPD-ADA mix as a pair of sets each including 48 different salts (No. 1-48 from Hampton Research HR2-245) at final concentrations of 0.1 and 0.4 M. The additive screen was prepared in the MPD-ADA mix using the Hampton Research HR2-138 kit (96 different additives) at 10% of its original concentration in the kit.

(iii) Broad pH Screen. To properly screen for pH dependence, 45 buffer conditions in the pH range from 2.2 to 11.0 were prepared at 0.1 M using the Hampton Research HR2-241 kit in 5 and 8% (v/v) MPD. Altogether, this resulted in the creation of six 96-condition screen kits (Figure 5) for use in combination with the host lipid screen. Further, the host lipid screens were performed at 4 and 20 °C. With six test host lipids and monoolein as a reference MAG and with screens evaluated in the forward and reverse directions,[7] this resulted in the setting up and evaluation of one hundred and sixty-eight 96-well plates. Given the magnitude of the effort involved and the fact that half of the plates had to be screened and scored manually in a walk-in refrigerator at 4 °C, it was important to have reduced the number of parameters that must be screened as early as possible in the exercise.

The host lipid screening study at 20 °C produced microcrystals alongside precipitated protein in 7.8, 9.7, and 8.8 MAG with biggest crystals appearing in 9.7 MAG (Figure 6A−C). No crystals were observed with 7.7, 7.9, and 8.9 MAG. At 4 °C, 7.9, 9.7, and 8.8 MAG generated microcrystals (Figure 6D−G), but nothing crystalline was observed with 7.7, 7.8, and 8.9 MAG. Likewise, the broad pH, salt, and additive screens were unsuccessful in supporting the growth of crystals that appeared visually any better than those observed under

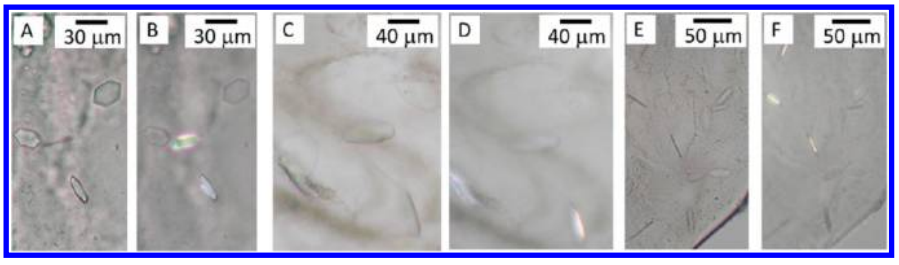

Figure 7. Effect of nitrate salts on the crystallization of mPGES1*. mPGES1* crystals grown at 4 °C in the presence of 0.1 M $NaNO_3$ (A, B), 0.4 M $NaNO_3$ (C, D), and 0.1 M NH_4NO_3 (E, F). Images were recorded with normal light (A, C, E) and between crossed polarizers (B, D, F) 5 days post setup. The hosting mesophase consisted of 5 mol % DOPC in 8.8 MAG. Ligands BI1 and BI2 were present in (C, D) and (E, F), respectively. The precipitant solutions contained 2 mM GSH, 8% (v/v) MPD, and 70 mM ADA pH 7.1.

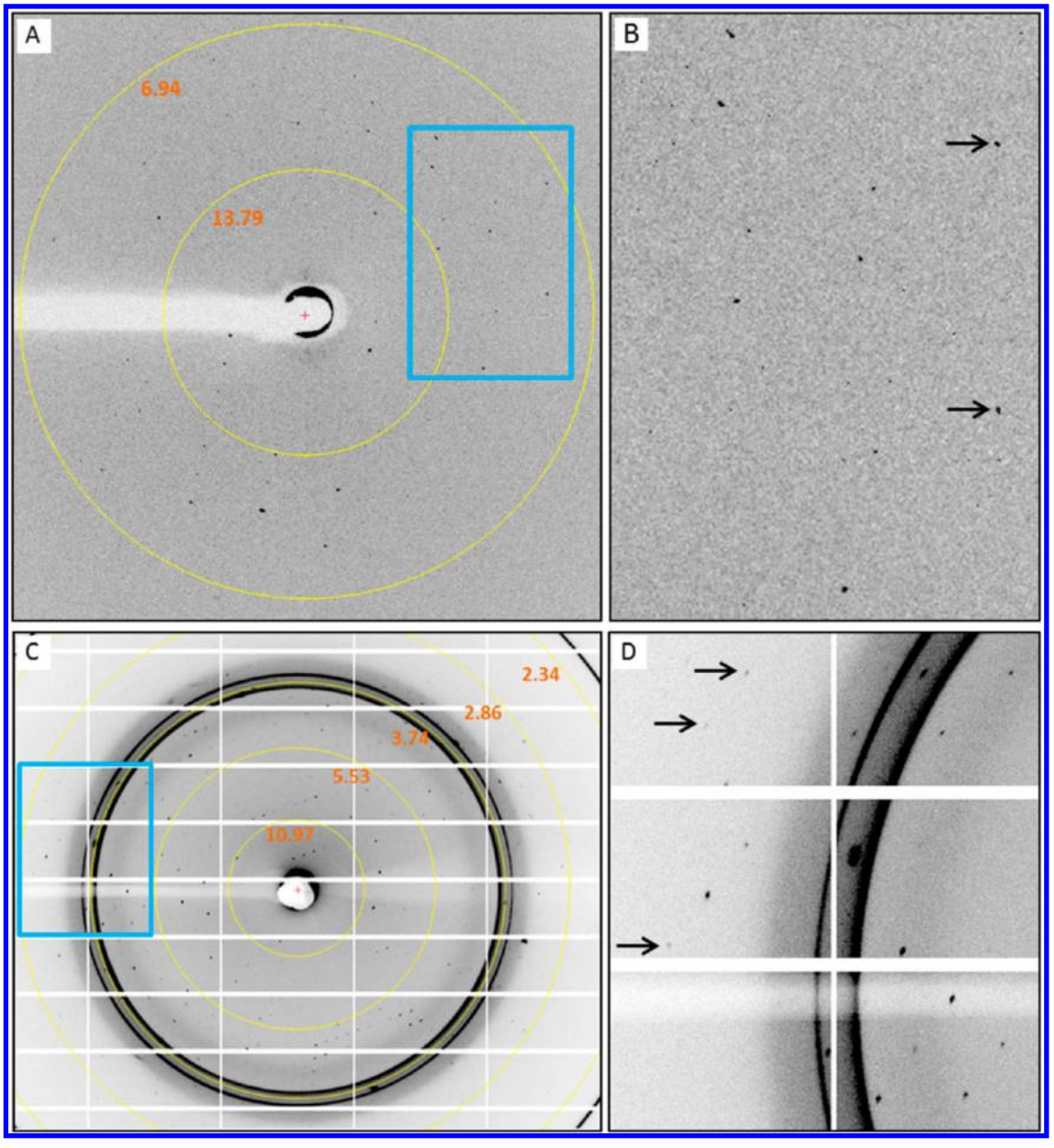

Figure 8. Diffraction from crystals of mPGES1* grown in nitrate-containing conditions. Diffraction pattern recorded with a crystal grown in the absence of ligand (A, B) at beamline 23ID-B, APS, and in the presence of ligand BI1 (C, D) at beamline I24, DLS. Rings indicating resolution (Å) are shown in yellow. Panel B and D are expanded views of boxed areas of panel A and C, showing reflection (arrows) to 7.0 Å and 3.0 Å, respectively. The sharp powder rings at about 3.7 Å originate from mesophase lipid that has crystallized.

reference conditions (sections 3.3.1 and 3.4.1; Figures 3 and 4). However, the MPD-pH grid screen provided some interesting results. First, the pH range that supported crystal growth changed depending on host lipid identity. Specifically, pH 6.7–

dx.doi.org/10.1021/cg500157x | *Cryst. Growth Des.* 2014, 14, 2034−2047

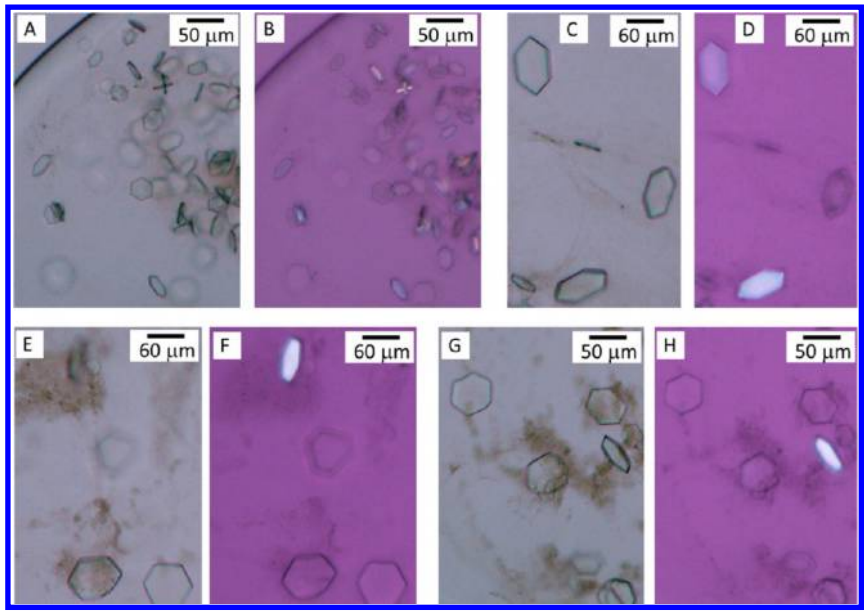

Figure 9. Additive lipid optimization of mPGES1* crystallization in 8.8 MAG at 4 °C with ligand BI2. (A, B) 5 mol % DOPC. (C, D) 0.5 mol % DOPC. (E, F) 1 mol % DOPC. (G, H) 2 mol % DOPC. Precipitant solutions contained 2 mM GSH, 8% (v/v) MPD, 0.4 M KNO_3, 0.1 M lithium citrate, and 70 mM ADA pH 7.1. Images were recorded with (B, D, F, H) and without crossed polarizers (A, C, E, G).

7.5 proved best for 7.8 and 7.9 MAG, pH 6.5−7.9 worked best for 9.7 MAG, and for 8.8 MAG the optimum was pH 6.3−7.9. Second, in 8.8 MAG different pH values gave rise to different crystal types (Figure 6F−H). Thus, needle-shaped crystals were obtained at pH 6.3−6.9, while small blocky crystal emerged at pH 7.1−7.9.

Following this round of screening, it was decided that 4 °C would be used for further optimization. This decision was arrived at because, in all of the host lipids tested, crystals tended to grow too quickly, generally producing showers of microcrystals and precipitated protein at the higher temperature. We next needed to choose a host lipid with which to proceed. Despite the fact that 9.7 MAG produced biggest crystals at 20 °C, the corresponding crystals at 4 °C were considerably smaller than those in 8.8 MAG at low temperature. For this reason, plus the fact that blocky crystals with a reasonably sized third dimension were observed with 8.8 MAG (Figure 6H), it was selected as the host lipid with which to pursue follow-up optimization. Because crystals were obtained most reproducibly in the pH range 6.7−7.3, this was chosen as the pH range for additional rounds of screening. Note that the original salt and additive screening was done at pH 6.5 (section 3.4.1). This is outside the chosen range and was considered suboptimal. Accordingly, it was decided to rescreen for salt and additive in the pH range 6.7−7.3.

3.4.3. Use of Ligands and Salt Screening at Optimal pH Values. To screen for salt and additives in the pH range from 6.7 to 7.3 (0.2 unit increments), four 96-well plates were set up that incorporated the following basic conditions: 70 mM ADA, 2 mM GSH, 8% (v/v) MPD, 8.8 MAG and 4 °C. Superimposed on this was a screen of protein concentration performed at 10, 15, 20, and 40 mg/mL in the solution used for mesophase self-assembly. At 40 mg/mL, a cubic-to-lamellar phase transition was triggered, most likely due to the high final DM concentration. The other protein concentrations produced crystals, but the biggest crystals were obtained at 20 mg/mL. It was selected therefore as the protein concentration for use in further optimizations.

mPGES1 is a potential drug target for which a number of high affinity inhibitor-type ligands are available. Two were investigated in the current study with a view to locking the protein into a single, stable conformation more amenable to crystallization. The ligand, BI1, has a K_i for mPGES1 of 2.4 nM and was provided as a solution in DMSO at 0.2 M. It was combined with the protein at 7 mM corresponding to a 7:1 mole ratio of ligand and protein about 30 min before reconstitution. The ligand did not dissolve fully in the aqueous protein solution. However, the aqueous dispersion that included precipitated ligand and protein was used directly for mesophase preparation. Following the usual reconstitution procedure, an optically clear mesophase was obtained that presumably had the ligand solubilized in the DOPC-doped 8.8 MAG bilayer of the mesophase and bound to the enzyme. This dispersion was then used to perform the salt and additive screen outlined above.

This set of trials confirmed that crystallization was more reproducible at pH 6.7 and 7.1. Further, nitrate was identified as a key component supporting the growth of significantly larger crystals than had been observed to date. These appeared with and without added ligand (Figure 7). Of note is the fact that nitrate was a key player in the DgkA project also. The crystals grown without ligand diffracted to 7.0 Å (Figure 8A,B). The addition of ligand improved the diffraction quality to 2.9 Å (Figure 8C,D). However, the mPGES1* crystals were quite radiation sensitive. This, plus their pronounced fragility, suggested that another round of optimization was in order.

3.4.4. The Value of a Second Salt. Given the dramatic effect nitrate had on crystal quality, it was decided to perform a second salt screen in the presence of nitrate with a view to identifying other beneficial salts. The screen was performed using salts from the Hampton kit HR2-245 at a concentration of 0.1 and 0.4 M in the presence of 0.4 M potassium nitrate, 8% (v/v) MPD, 2 mM GSH, 70 mM ADA at pH 6.7 and pH 7.1. This took the form of two additional 96-condition screen kits used with 8.8 MAG at 4 °C. Lithium citrate at 0.1 M generated 30 μm-sized hexagonal crystals (Figure 9A) in the presence of

dx.doi.org/10.1021/cg500157x | *Cryst. Growth Des.* 2014, 14, 2034−2047

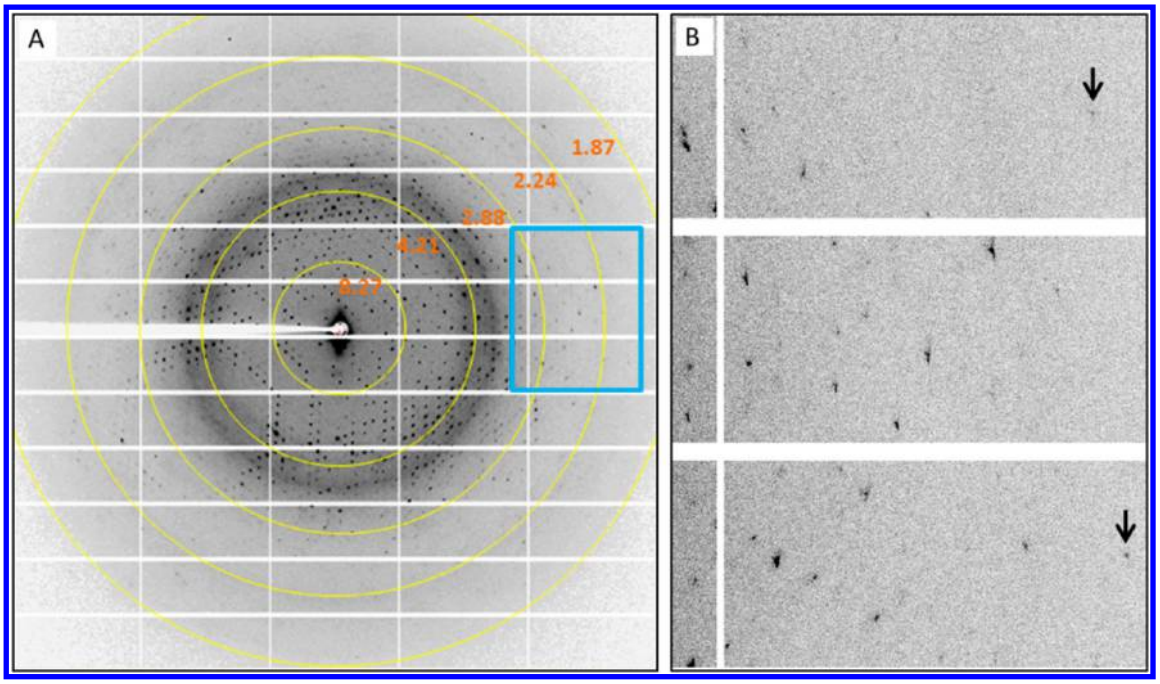

Figure 10. Diffraction from mPGES1* crystals grown in 8.8 MAG doped with 1 mol % DOPC in the presence of ligand BI1. (A) Diffraction pattern recorded at beamline PXII, SLS, with a 10-fold attenuated 10 × 15 μm^2 beam. The sample-to-detector distance was set to 350 mm. (B) Zoomed-in view of the boxed area in (A) showing diffraction spots to 2.08 Å (arrows).

the ligand BI2 (K_i, 3.8 nM). Importantly, the crystals were noticeably thicker than those observed in its absence (Figure 7). Further optimization trials, which included changing the concentration of the two salts, as well as MPD and GSH, did not improve crystal size.

3.4.5. DOPC Concentration. As noted (section 3.3.1) DOPC at 5 mol % proved instrumental in the production of initial hits. However, 5 mol % represented an arbitrary figure with which to initiate the project. It seemed appropriate at this juncture to explore the effect other concentrations of DOPC would have on the crystallization outcome. Accordingly, DOPC at 0.5, 1, and 2 mol % in 8.8 MAG was evaluated under conditions optimized to this point in the presence of ligand. Best quality crystals, as judged by eye, were observed at 0.5 and 1 mol % DOPC (Figure 9). Crystals grown at 1 mol % were harvested and tested at Beamline PXII, Swiss Light Source, Switzerland. A diffraction pattern is shown in Figure 10. A complete data set to a resolution of 2.08 Å was obtained with a single crystal without changing the location along the crystal. At the time the data were collected, an X-ray crystal structure of mPGES1 was not available.[6] The structure was solved by sulfur single-wavelength anomalous diffraction (S-SAD). Details of the S-SAD experiment and of the liganded structure will be reported on separately.

4. DISCUSSION

Crystal Design. The mPGES1* construct used in this study was designed to reproduce crystal contacts observed with LTC4S, a structural homologue of mPGES1. Modeling the C-terminal α-helical extension of LTC4S onto the 3.5 Å electron crystallographic structure of mPGES1 (PDB ID 3DWW) suggested that it might be possible to reproduce these LTC4S crystal contacts (Figure 1). Alas, the mPGES1* protein (which included 21 C-terminal residues from LTC4S) did not give crystals that reproduced the LTC4S crystal contacts. However, to some degree, the original objective was realized in that a high resolution structure was obtained for mPGES1* with crystal contacts dominated by the C-terminal fusion peptide. However, the fusion peptide in mPGES1* adopted a conformation quite unlike the α-helical extension in LTC4S we had hoped to replicate (Figure 11). It consists of a three-residue turn (Phe152-Pro154), an eight-residue α-helix (Ala155-Leu162), and a nine-residue coil (Gly163-Trp171, Ala172 does not show in density). This C-terminal *t*urn-*h*elix-*c*oil (THC) forms a number of contacts that hold the crystal together (Figure 12). As expected, for crystals grown by the in meso method, packing

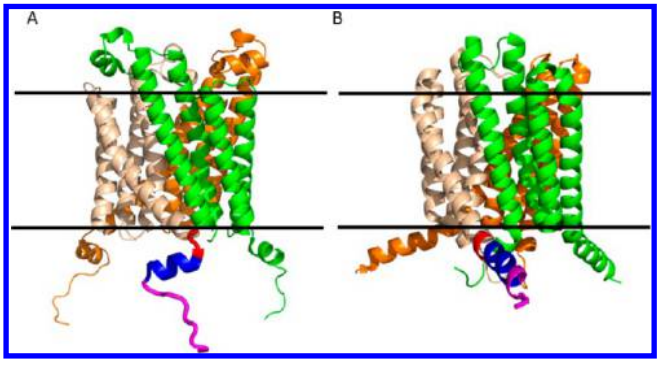

Figure 11. Structure comparison of mPGES1* and LTC4S highlighting the marked difference in conformation at the C-terminus. (A) mPGES1* (PDB ID 4BPM, 2.08 Å, this work). (B) LTC4S[27] (PDB ID 2UUH, 2.15 Å). Each enzyme consists of a trimer. Monomers are colored cream, green and brown. The C-terminus in one of the monomers in (A) is color-coded according to conformation type corresponding to the THC designation in mPGES1* as follows: turn (Phe152-Pro154), red; helix (Ala155-Leu162), blue; coil (Gly163-Trp171), magenta. To facilitate comparison, a similar color coding has been applied to the C-terminus of LTC4S. The approximate locations of the endoplasmic reticulum membrane boundaries are marked by horizontal lines (blue, lumen side; red, cytoplasmic side).

dx.doi.org/10.1021/cg500157x | *Cryst. Growth Des.* 2014, 14, 2034−2047

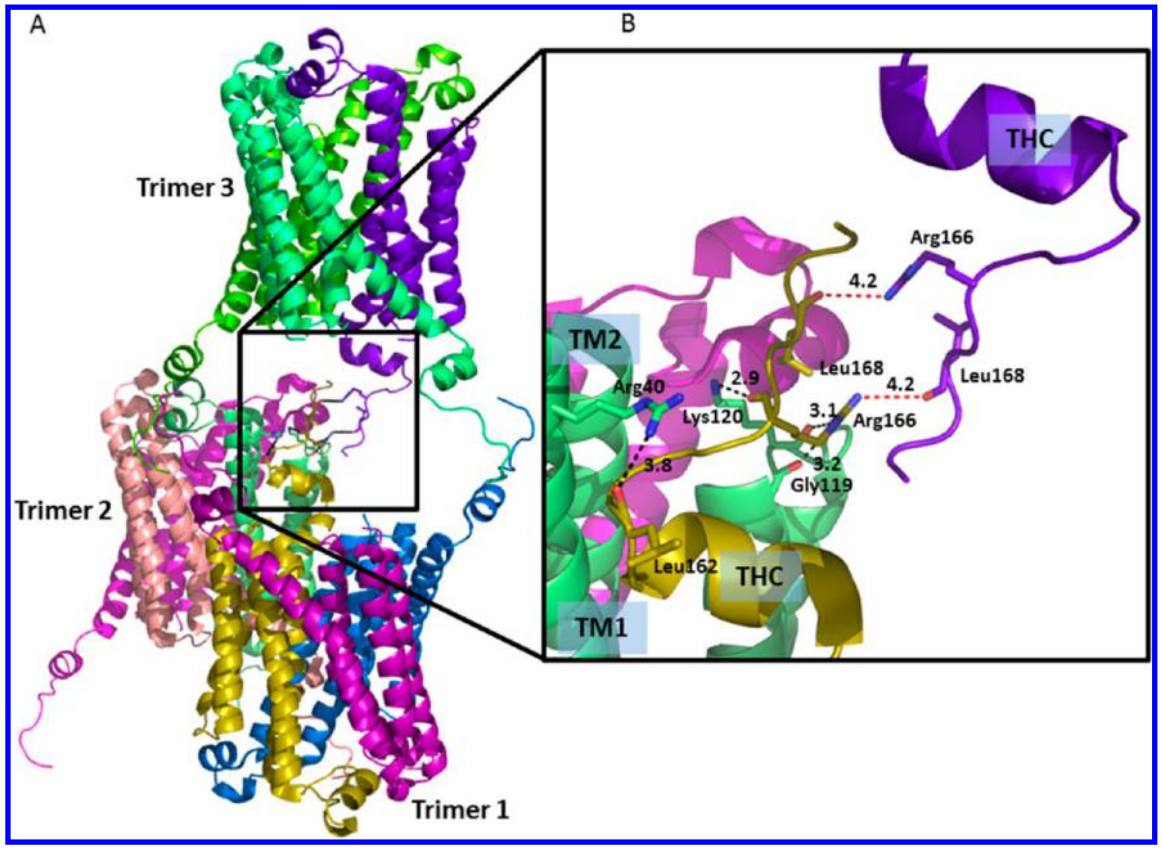

Figure 12. Crystal contacts in mPGES1* that involve the C-terminal fusion peptide. (A) Three trimers of mPGES1* are shown for context. Trimers 1 and 2 reside within the same layer in the crystal which is of Type 1. Trimer 3 is in an adjacent layer. (B) An expanded view of the boxed area in (A). All interactions (dashed lines), corresponding to contacts of <4.5 Å, that involve a single C-terminal THC segment (yellow monomer) are identified. The total number of interactions is six. Four originate from Arg166; the other two involve Leu162 and Leu168. Interactions that involve THC exist within and between layers. Distances are shown in Å. TM1 and TM2 refer to transmembrane helices.

is layered or Type I. Crystal contacts formed by THC exist both within and between layers and no doubt contribute to lattice stability.

It is worthwhile speculating as to why the fusion peptide adopts such dissimilar conformations in LTC4S and mPGES1*. For one, the methods used to crystallize the two proteins are entirely different. One used protein−detergent complexes and the in surfo method at 20 °C. The other used protein reconstituted into a lipid bilayer of the cubic phase and the in meso method at 4 °C. The physical and chemical environments are, accordingly, profoundly different, and this may account for the different conformations and crystal contacts. The precipitants used with the two targets are also dissimilar. For LTC4S, the precipitant contained 0.1 mM GSH, 2% (v/v) PEG 400, 2 M ammonium sulfate, and 100 mM HEPES-Na pH 7.5.[27] For mPGES1*, the precipitant had 2 mM GSH, 0.4 M potassium nitrate, 0.1 M lithium citrate, and 70 mM ADA, pH 7.1. Of course, the proteins to which the fusion peptide is attached are completely different. And thus, despite the 11% identity and 32% similarity in sequence, and the aforementioned structural homology, the influence of the nature of the integral membrane anchor may extend into the THC peptide in a way that stabilizes an anchor-specific conformation.

Despite the goal of rational design not being realized, it is possible that the fusion peptide used here may prove generally useful. The logic behind its use with mPGES1 was to provide extramembranal bulk to a protein that, for the most part, is integral to the membrane, and well-structured interhelical crystal contacts. While the helix conformation did not materialize, the THC extension nevertheless did the job in that it provided crystals contacts and a high-resolution structure. It is apparent that THC can adopt different contact-forming conformations depending on context. To date, we only have two contexts upon which to base this statement. However, if it is transferable then this same THC extension, or a variation of it, might be used to advantage with other membrane proteins that, like mPGES1, are hydrophobic with little extramembranal bulk. Where THC should be appended would, of course, depend on the target. Because of its extended conformation, the C- or N-termini are obvious points of attachment. THC includes at least two helix destabilizing residues, Pro154 and Gly163, respectively at the beginning and end of the helical segment. Obviously, these can exist also within a helix, as in LTC4S. Thus, keeping them as part of the fusion peptide for use with other targets makes sense in that they should provide for conformational flexibility thus widening the range of targets with which this strategy works. A somewhat related approach of using different fusion proteins and appending them to different parts of the target protein has been implemented successfully within the GPCR family.[2]

Additive Phospholipids. In meso crystallogenesis, which takes place in or from a lipidic mesophase, provides an opportunity to screen and to optimize the process on the basis of the lipids that make up the mesophase. These come in two forms, host and additive lipids. The host lipid is responsible for forming the membrane fabric that permeates the mesophase.

dx.doi.org/10.1021/cg500157x | Cryst. Growth Des. 2014, 14, 2034−2047

Additive lipids can be used to dope the host mesophase to several ends. These range from stabilizing the target membrane protein in a functional form[33] to altering the microstructure and transport properties of the mesophase itself in a way that facilitates nucleation and crystal growth. In this study, added PC proved crucial to the successful crystallization and structure determination of mPGES1*. The first crystal hit, after considerable preliminary prescreening had been performed, was obtained when the host lipid was doped with 5 mol % DOPC. This initial hit formed the basis of subsequent rounds of screening and optimization that eventually led to a structure. A further refinement identified 1 mol % DOPC as the optimum and the concentration used for a final structure determination. Interestingly, PC molecules were not visible in the crystal structure.

Additive lipids have been used to advantage in the GPCR arena.[2] Thus, cholesterol, in the 8−12 mol % range, are routinely combined with the host MAG to help crystallize receptors and receptor complexes.[2] In many cases, cholesterol appears as part of the final structure. Likewise, with sensory rhodopsin, native phospholipids from *Halobacterium salinarum* have proven critical as additives in the crystallization and structure determination of this light sensing proton pump.[34]

With the in surfo crystallization method too, added phospholipid can mean the difference between crystals and no crystal. Further, dramatic improvements in crystal quality that lead to structure determination are attributed to lipid augmentation.[35−37]

Host Lipids. As of this writing, 161 structure records have been reported in the PDB that are attributed to the in meso crystallization method. The vast majority (145) of these were crystallized with 9.9 MAG as the host lipid. Of the others, bacteriorhodopsin was crystallized with the β-XylOC$_{16+4}$ lipid,[38] sensory rhodopsin II−transducer complex[39] and gramicidin[40] were crystallized with 11.7 MAG, and the remaining nine with shorter chain MAGs. The latter included 7.7 MAG for caa_3 cytochrome oxidase,[41] the β_2 adrenergic receptor-Gs complex,[4] and an active β_2 adrenergic-nanobody complex,[42] 7.8 MAG for DgkA,[43] 7.8 MAG for the alginate transporter,[44] and 7.7 and 8.8 MAG for gramicidin.[2,40] To this list we can now add mPGES1* in 8.8 MAG. For most of these targets, the particular short chain MAG in question was essential to the success of the project by enabling crystallization in the first instance and/or improving crystal quality to the point of providing a useful structure.

With these data in hand, it is reasonable to ask if any recommendations can be made with regard to choosing a particular MAG or set of MAGs with which to perform in meso crystallization trials. For GPCRs, 9.9 MAG has been hugely successful and is the host lipid of choice. However, GPCRs in complex with other proteins, G proteins and nanobodies to date, are best crystallized in 7.7 MAG.[4,42] More generally, it is hard to give specific recommendations other than to strongly encourage performing a host lipid screen when the lipid under investigation is not working. Further, the need to be persistent and expansive in the performance of such screening trials cannot be overstressed. The latter recommendation derives, in part, from experience gained in the current study. The project started with 9.9 MAG and, for lack of success, moved on to 7.8 MAG. But this short chain lipid only gave small crystals at 20 °C. Expanding the screen to include a total of five additional host lipids eventually led to 8.8 MAG and to structure-yielding crystals at 4 °C.

Until quite recently, these alternative MAGs had been synthesized and purified in-house. Given their proven general usefulness and success with high profile targets,[4,42] several (7.7, 7.8, 7.9, 8.6, 8.7, 8.8, and 9.7 MAG) are now available commercially. While these alternative MAGs are expensive, the fact that they are more generally available means they will be tested with diverse targets. As the database of in meso structures grows, data mining should provide guidelines for rationally choosing host lipids based on a target's homology with a solved structure or a predicted membrane topology.

MAG-Dependent Precipitants. Having gained so much experience with 9.9 MAG over the years, the precipitants that are compatible and that have proven successful with it as a host lipid are reasonably well established. With other MAGs, much less information is available. However, having now worked on seven different membrane proteins (OprB, cytochrome oxidase, the β_2 adrenoreceptor-Gs complex, AlgE, DgkA, PepT and gramicidin) in three different host MAGs (7.7, 7.8, 8.8), some general guidelines are beginning to emerge regarding the type and concentration of precipitant components to use with particular host lipids. PEG and MPD will be used as examples here. Both figure prominently in the list of precipitant components that support the generation of structure-quality crystals. And both induce, in a concentration-dependent manner, a swelling of the cubic phase and its eventual transformation to the sponge phase.[45,46] Because the cubic and sponge phases are bicontinuous, crystallization can take place in either. However, beyond a certain PEG or MPD concentration the sponge phase is destabilized and can convert entirely to the lamellar phase. To our understanding, the bulk lamellar phase does not support the growth of macroscopic crystals by the in meso method.[48] With different host lipids, the precipitant concentration dependence of these assorted effects changes. Thus, when resources permit, the full range of PEG 400 and MPD concentrations should be screened with each host lipid. However, should resources be limited, we recommend using 8−16% (v/v) MPD and 34−42% (v/v) PEG 400 for MAGs with acyl chains 17 and 18 carbon atoms long. For MAGs with chains 14 and 15 carbons long, these two concentration ranges should be halved. Intermediate concentrations can be used with MAGs having chains 16 carbon atoms long.

The above discussion refers to the response of the mesophase to precipitant components. It is necessary also to consider how the protein itself reacts to these crystallants in the context of nucleation and crystal growth. In practice, the two responses are coupled and the consequences of using a given precipitant component at a particular concentration will depend on the identity of the target protein and that of the host MAG. Nonetheless, on the basis of our limited experience with bacteriorhodopsin,[9] OprB,[7] PepT (unpublished), and DgkA[8] shorter chain MAGs generally support the growth of structure-yielding crystals when used with precipitant components at lower rather than higher concentrations.

Lessons Learned. To date, two detailed studies of in meso crystallization of integral membrane proteins that make use of hosting lipids, as implemented in the MS&FB group, have been reported. The first referred to a β-barrel outer membrane porin, OprB. The second, DgkA, an α-helical trimeric kinase. Given the α-helical nature of mPGES1, it made sense to implement the strategy that worked with DgkA to this new target. An obvious question to ask then is, did the strategy work in the sense of shortening the time, reducing the number of screens

performed, and so on, in going from pure protein to final structure? The answer is a resounding yes. The DgkA project lasted 3 years and involved/required the following: in excess of 30 protein preparations, over 4000 96-well plates screened at 4 °C, 82 optimization screens designed and tested, and ∼2800 crystals evaluated for diffraction over 35 synchrotron trips. By contrast, the mPGES1* project involved six protein purification preparations, ∼300 crystallization plates, 18 optimization screens designed and tested, and 4 synchrotron trips during which ∼100 crystals were evaluated for diffraction. From mPGES1* purification to solved structure took ∼8 months. While the comparison is not entirely systematic and the two projects diverge in several ways, both were carried out in the same lab, driven by the same lead researcher (D.L.) with approximately the same resources at hand, and both projects were mostly realized in the cold room at 4 °C. The data, while limited, do suggest that there was an improvement in the efficiency of the process. Obviously lessons had been learned from the original DgkA work, and indeed from the OprB project which incidentally was also directed by D.L. Parenthetically, we note that, despite the efficiency just referred to, we were well "beaten to the post" in that an in surfo structure to 1.2 Å resolution for mPGES1 was published not long after we obtained a structure for mPGES1*.[6] The lesson, to not rely on a single crystallization method, is painfully obvious.

An argument could be advanced that DgkA and mPGES1 are similar targets and that it is not unreasonable for the strategy that worked with one to work with the other. To a degree the targets are similar in that both are relatively small α-helical trimers. Nonetheless, the lessons learned from both with regard to crystallogenesis are likely to find general applicability. Below, we list these lessons in no particular order of priority.

Numbers. It is important to be prepared to set up and to screen a large number of conditions. The numbers reported in this work can be used for calibration purposes. Fortunately, in meso crystallization is highly efficient and requires very small amounts of protein and lipid.

Temperature. Perform trials initially at 20 °C. At the very least, 4 °C should be tested next. Because the cubic mesophase readily undercools, 9.9 MAG, and the other MAGs in our experience, can be used in screens at 4 °C.

Host Lipid. Begin with 9.9 MAG unless you have prior knowledge that a different MAG is preferred. As needed, explore short chain MAGs. A large number are now available commercially. We would typically test 7.7, 7.8, 7.9, 9.7 and 8.8, in that order.

Additive Lipid. The choice of lipid is dictated by the target and prior knowledge in relation to its preferences regarding stability and function. To date cholesterol, DOPC, and native phospholipids have been used successfully. Not only should the identity of the lipid be examined but also the concentration at which it is used. Further, the method of adding the lipid needs to be considered. With mPGES1*, adding it to the host lipid prior to reconstitution worked; adding it to the protein prior to reconstitution did not.

pH. Perform a wide pH screen as early in the process as possible. Try to avoid cacodylate which contains the toxic and strongly X-ray absorbing and fluorescing heavy atom arsenic. If phosphate or other such buffers are used that are known to form insoluble salt crystals with cations such as calcium and magnesium, carefully check that early stage crystals are indeed made of protein.

Protein Concentration. This should be screened for early on in the process. Use the highest protein concentration available and dilutions of same. If detergent carry-over is excessive, the higher protein concentrations tested could destabilize the cubic phase, as observed with mPGES1*.

Salts. Perform this screen as described under Methods at a final concentration of 0.1 and 0.4 M. A second, and perhaps even a third, salt screen later in the screening/optimization process can prove invaluable in the identification of additional salt components that will progress the project toward a structure. A second salt screen proved crucial to the success of the mPGES1* study.

Additives. Small diols, such as butanediol and hexanediol, help drive the mesophase in the direction of the sponge phase. This has been found to increase crystal size, especially when the mesophase is not in the sponge phase to begin with. In our experience, organic solvents, such as the alcohols and acetone, as found in the Hampton Research Additive screen kit, are not useful for in meso crystallogenesis.

Precipitants. The precipitants used to date with the in meso method fall into two major categories. The first consists of polymers and polyols with the potential to spongify the lipidic mesophase. Specific examples include PEG 400 (GPCRs), Jeffamine M600 (photosynthetic reaction centers), pentaerythritol propoxylate (light harvesting complex II), and MPD (cobalamin transporter, BtuB, DgkA, and mPGES1*). The second employ a high concentration of salts. Examples include sodium/potassium phosphate for bacteriorhodopsin and sodium acetate for AlgE. Given the diversity of the precipitants that have worked across all crystallization methods, it is still recommended that a broad initial screening should be performed with commercial kits such as the ones reported in this paper. As the database of in meso-based structures grows, particular types of screens will emerge for specific target types. A good example of this is the PEG 400-based screens that are proving highly successful with GPCRs.[47]

Ligand. If the apo form of the target proves refractory to crystallogenesis, tight binding ligands, where available, can prove invaluable. This is well proven with GPCRs where every published structure is of a liganded complex. Often these are added during protein expression and purification. If the ligand (thermally) stabilizes the target, this is all the more reason for including it because stability and crystallizability would appear to be strongly positively correlated.

Constructs. Protein engineering can be hugely beneficial in the realization of a crystal structure. Both DgkA and mPGES1*, as is the entire set of GPCRs, are cases in point. Engineering can be done to stabilize the target, to provide crystal contacts, to prevent post-translational modification, and to remove segments, disordered termini or loops for example, that may interfere with crystallization. With all such modifications, it is important to evaluate the effect the changes have on function.

AUTHOR INFORMATION

Corresponding Author

*Phone: 353-1-896-4253. Fax: 353-1-896-4253. E-mail: martin.caffrey@tcd.ie. Web: http://www.tcd.ie/Biochemistry/research/m_caffrey.php.

Notes

The authors declare no competing financial interest.

■ ACKNOWLEDGMENTS

The authors thank Drs. L. Vogeley and J. Lyons, for help with diffraction data collection and A. Löhle for initial support in protein purification. This work was supported by grants from Science Foundation Ireland (12/IA/1255) and the National Institutes of Health (GM75915, P50GM073210, U54GM094599). X-ray diffraction data were collected on the I24 beamline at the Diamond Light Source, Didcot, Oxford, UK, and the PX II and PX III beamlines at the Swiss Light Source, Villigen, Switzerland.

■ REFERENCES

(1) Caffrey, M. *J. Struct. Biol.* **2003**, *142*, 108−132.
(2) Caffrey, M.; Li, D.; Dukkipati, A. *Biochemistry* **2012**, *51*, 6266−6288.
(3) Landau, E. M.; Rosenbusch, J. P. *Proc. Natl. Acad. Sci. U. S. A.* **1996**, *93*, 14532−14535.
(4) Rasmussen, S. G.; DeVree, B. T.; Zou, Y.; Kruse, A. C.; Chung, K. Y.; Kobilka, T. S.; Thian, F. S.; Chae, P. S.; Pardon, E.; Calinski, D.; Mathiesen, J. M.; Shah, S. T.; Lyons, J. A.; Caffrey, M.; Gellman, S. H.; Steyaert, J.; Skiniotis, G.; Weis, W. I.; Sunahara, R. K.; Kobilka, B. K. *Nature* **2011**, *477*, 549−555.
(5) Jegerschold, C.; Pawelzik, S. C.; Purhonen, P.; Bhakat, P.; Gheorghe, K. R.; Gyobu, N.; Mitsuoka, K.; Morgenstern, R.; Jakobsson, P. J.; Hebert, H. *Proc. Natl. Acad. Sci. U. S. A.* **2008**, *105*, 11110−11115.
(6) Sjogren, T.; Nord, J.; Ek, M.; Johansson, P.; Liu, G.; Geschwindner, S. *Proc. Natl. Acad. Sci. U. S. A.* **2013**, *110*, 3806−3811.
(7) Li, D.; Lee, J.; Caffrey, M. *Cryst. Growth Des.* **2011**, *11*, 530−537.
(8) Li, D.; Shah, S. T. A.; Caffrey, M. *Cryst. Growth Des.* **2013**, *13*, 2846−2857.
(9) Misquitta, L. V.; Misquitta, Y.; Cherezov, V.; Slattery, O.; Mohan, J. M.; Hart, D.; Zhalnina, M.; Cramer, W. A.; Caffrey, M. *Structure* **2004**, *12*, 2113−2124.
(10) Coleman, B. E.; Cwynar, V.; Hart, D. J.; Havas, F.; Mohan, J. M.; Patterson, S.; Ridenour, S.; Schmidt, M.; Smith, E.; Wells, A. J. *Synlett* **2004**, *2004*, 1339−1342.
(11) Caffrey, M., Lyons, J. A., Smyth, T., Hart, D. J. In *Current Topic in Membranes*; DeLucas, L., Ed.; Academic Press: Burlington, 2009; pp 83−108.
(12) Li, D.; Boland, C.; Walsh, K.; Caffrey, M. *J. Vis. Exp.* **2012**, *67*, e4000.
(13) Cheng, A.; Hummel, B.; Qiu, H.; Caffrey, M. *Chem. Phys. Lipids* **1998**, *95*, 11−21.
(14) Cherezov, V.; Clogston, J.; Misquitta, Y.; Abdel-Gawad, W.; Caffrey, M. *Biophys. J.* **2002**, *83*, 3393−3407.
(15) Cherezov, V.; Peddi, A.; Muthusubramaniam, L.; Zheng, Y. F.; Caffrey, M. *Acta Crystallogr. D* **2004**, *60*, 1795−1807.
(16) Li, D.; Boland, C.; Aragao, D.; Walsh, K.; Caffrey, M. *J. Vis. Exp.* **2012**, *67*, e4001.
(17) Kabsch, W. *Acta Crystallogr. D* **2010**, *66*, 125−132.
(18) Collaborative Computational Project N.. *Acta Crystallogr. D* **1994**, *50*, 760−763.
(19) Schneider, T. R.; Sheldrick, G. M. *Acta Crystallogr. D* **2002**, *58*, 1772−1779.
(20) McCoy, A. J.; Grosse-Kunstleve, R. W.; Adams, P. D.; Winn, M. D.; Storoni, L. C.; Read, R. J. *J. Appl. Crystallogr.* **2007**, *40*, 658−674.
(21) Cowtan, K. *Joint CCP4 and ESF-EACBM Newsl. Protein Crystallogr.* **1994**, *31*, 34−38.
(22) Cowtan, K. *Acta Crystallogr. D* **2006**, *62*, 1002−1011.
(23) Emsley, P.; Lohkamp, B.; Scott, W. G.; Cowtan, K. *Acta Crystallogr. D* **2010**, *66*, 486−501.
(24) Adams, P. D.; Afonine, P. V.; Bunkoczi, G.; Chen, V. B.; Davis, I. W.; Echols, N.; Headd, J. J.; Hung, L. W.; Kapral, G. J.; Grosse-Kunstleve, R. W.; McCoy, A. J.; Moriarty, N. W.; Oeffner, R.; Read, R. J.; Richardson, D. C.; Richardson, J. S.; Terwilliger, T. C.; Zwart, P. H. *Acta Crystallogr. D* **2010**, *66*, 213−221.
(25) Jakobsson, P. J.; Morgenstern, R.; Mancini, J.; Ford-Hutchinson, A.; Persson, B. *Protein Sci.* **1999**, *8*, 689−692.
(26) Holm, P. J.; Bhakat, P.; Jegerschold, C.; Gyobu, N.; Mitsuoka, K.; Fujiyoshi, Y.; Morgenstern, R.; Hebert, H. *J. Mol. Biol.* **2006**, *360*, 934−945.
(27) Martinez Molina, D.; Wetterholm, A.; Kohl, A.; McCarthy, A. A.; Niegowski, D.; Ohlson, E.; Hammarberg, T.; Eshaghi, S.; Haeggstrom, J. Z.; Nordlund, P. *Nature* **2007**, *448*, 613−616.
(28) Ago, H.; Kanaoka, Y.; Irikura, D.; Lam, B. K.; Shimamura, T.; Austen, K. F.; Miyano, M. *Nature* **2007**, *448*, 609−612.
(29) Ferguson, A. D.; McKeever, B. M.; Xu, S.; Wisniewski, D.; Miller, D. K.; Yamin, T. T.; Spencer, R. H.; Chu, L.; Ujjainwalla, F.; Cunningham, B. R.; Evans, J. F.; Becker, J. W. *Science* **2007**, *317*, 510−512.
(30) Davison, S. C.; Wills, E. D. *Biochem. J.* **1974**, *140*, 461−468.
(31) Hopkins, F. G. *Biochem. J.* **1921**, *15*, 285−305.
(32) Qiu, H.; Caffrey, M. *Biomaterials* **2000**, *21*, 223−234.
(33) Bogdanov, M.; Mileykovskaya, E.; Dowhan, W. *Subcell. Biochem.* **2008**, *49*, 197−239.
(34) Luecke, H.; Schobert, B.; Lanyi, J. K.; Spudich, E. N.; Spudich, J. L. *Science* **2001**, *293*, 1499−1503.
(35) Guan, L.; Smirnova, I. N.; Verner, G.; Nagamori, S.; Kaback, H. R. *Proc. Natl. Acad. Sci. U. S. A.* **2006**, *103*, 1723−1726.
(36) Zhang, H.; Kurisu, G.; Smith, J. L.; Cramer, W. A. *Proc. Natl. Acad. Sci. U. S. A.* **2003**, *100*, 5160−5163.
(37) Gourdon, P.; Andersen, J. L.; Hein, K. L.; Bublitz, M.; Pedersen, B. P.; Liu, X.-Y.; Yatime, L.; Nyblom, M.; Nielsen, T. T.; Olesen, C.; Møller, J. V.; Nissen, P.; Morth, J. P. *Cryst. Growth Des.* **2011**, *11*, 2098−2106.
(38) Borshchevskiy, V.; Moiseeva, E.; Kuklin, A.; Büldt, G.; Hato, M.; Gordeliy, V. *J. Cryst. Growth* **2010**, *312*, 3326−3330.
(39) Gordeliy, V. I.; Labahn, J.; Moukhametzianov, R.; Efremov, R.; Granzin, J.; Schlesinger, R.; Buldt, G.; Savopol, T.; Scheidig, A. J.; Klare, J. P.; Engelhard, M. *Nature* **2002**, *419*, 484−487.
(40) Hofer, N.; Aragao, D.; Lyons, J. A.; Caffrey, M. *Cryst Growth Des* **2011**, *11*, 1182−1192.
(41) Lyons, J. A.; Aragao, D.; Slattery, O.; Pisliakov, A. V.; Soulimane, T.; Caffrey, M. *Nature* **2012**, *487*, 514−518.
(42) Ring, A. M.; Manglik, A.; Kruse, A. C.; Enos, M. D.; Weis, W. I.; Garcia, K. C.; Kobilka, B. K. *Nature* **2013**, *502*, 575−579.
(43) Li, D.; Lyons, J. A.; Pye, V. E.; Vogeley, L.; Aragao, D.; Kenyon, C. P.; Shah, S. T.; Doherty, C.; Aherne, M.; Caffrey, M. *Nature* **2013**, *497*, 521−524.
(44) Tan, J.; Rouse, S. L.; Li, D.; Pye, V. E.; Vogeley, L.; Brinth, A. R.; Whitney, J. C.; Howell, P. L.; Sansom, M. S. P.; Caffrey, M. *Acta Crystallogr. D* **2014**, *70*, DOI: 10.1107/S1399004714001850.
(45) Ridell, A.; Ekelund, K.; Evertsson, H.; Engström, S. *Colloids Surf., A* **2003**, *228*, 17−24.
(46) Cherezov, V.; Clogston, J.; Papiz, M. Z.; Caffrey, M. *J. Mol. Biol.* **2006**, *357*, 1605−1618.
(47) Xu, F.; Liu, W.; Hanson, M. A.; Stevens, R. C.; Cherezov, V. *Cryst. Growth Des.* **2011**, *11*, 1193−1201.
(48) Caffrey, M. *Cryst. Growth Des.* **2008**, *8*, 4244−4254.